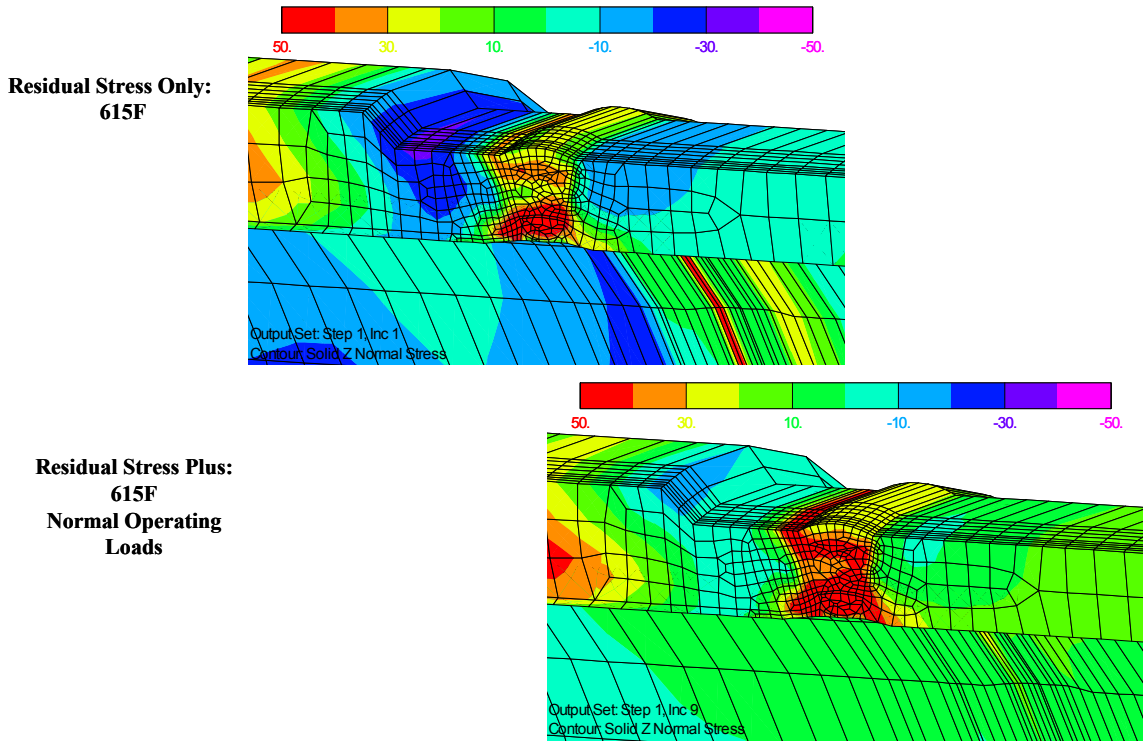

Figure G.50 Hoop stresses – used for FEAM analyses: outside weld first then inside weld

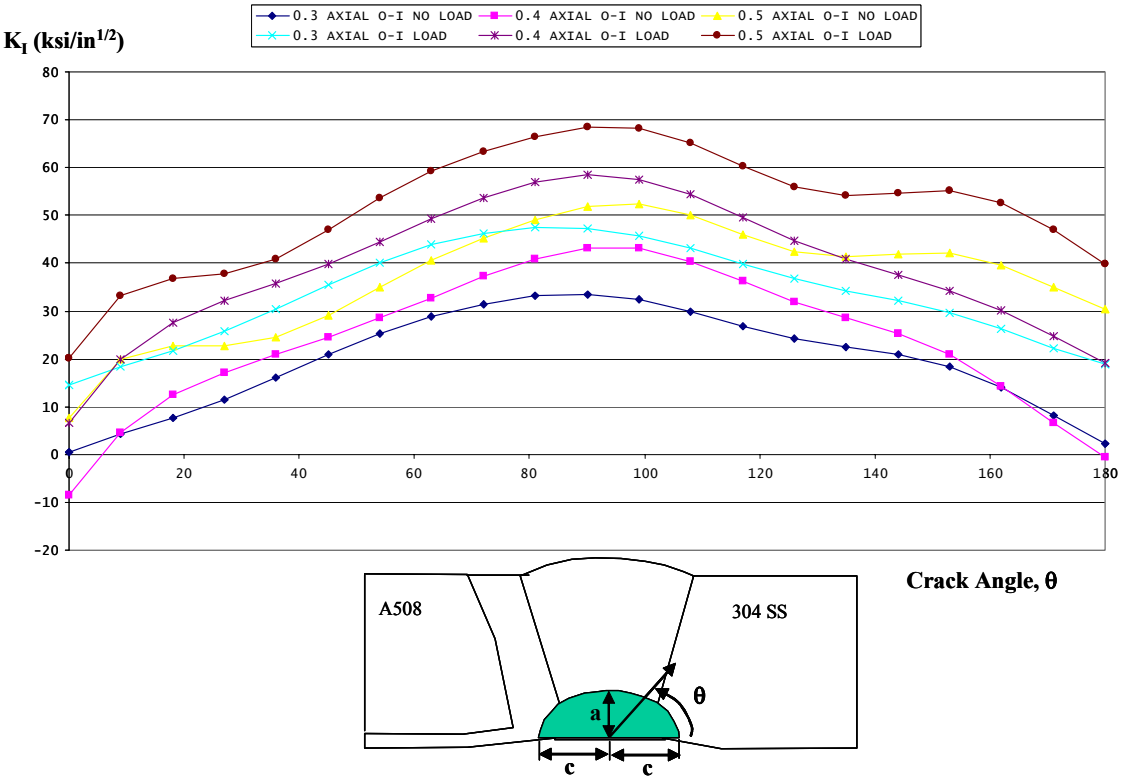

Figure G.51 Stress intensity factors; a = 0.3, 0.4, 0.5; c/a = 1.5. 'NO LOAD' = 'Residual Stress Only', 'LOAD' = 'Residual Stress Plus Normal Operating Load'

versa) depending on the welding process, it is important to model the welding process as well as the pipe geometry and multi-axial loading.

For these analyses, two weld processes were studied. In the first, the weld was assumed to start from the inner diameter and proceed to the outer surface. This is denoted Inside-Out or I-O. The second was the reverse process, denoted Outside-In or O-I, where the weld was completed from the outside and then the inside weld was deposited. All results presented in Figures G.52 through G.55 use this designation in the description above the illustration. Using the results of the finite element analysis we can impose a residual stress field on the calculated results. Both I-O and O-I were considered since it is not known how the actual hot leg in the V. C. Summer plant was repair welded (see the discussion related to Figure G.22).

Once the residual stress field has been calculated, the applied loading is modeled, the FRACALT code is used to determine the stress intensity factors, K, for a pre-defined set of crack sizes and orientations. These values of K are then normalized by $a^{1/2}$, where 'a' is the crack depth. A table of these normalized K values was then sent to the probabilistic mechanics code TRACLIFE and the surface crack changes during PWSCC growth calculated using the above equation. For the purpose of this analysis, it was assumed that the value of K along the crack drove the growth and shape. TRACLIFE was selected for the analysis because it has already built into the program the necessary 3D calculation tools. In addition, it is possible to examine the impact of uncertainty on these calculations at a later time.

The first case examined was the Inside-Out weld process. Because the residual stress field can lead to crack growth, **given that a crack exists**, two sets of calculations were performed. In the first, only the residual stresses were included. The second set of calculations added the applied loading. Note that the applied loading included the history of the entire weld process, and plasticity was included in the analysis.

It is critical to remember that the calculations were started with an assumed crack depth of 5 mm (0.20 inches). The question of initiation times and subsequent growth to the point at which the crack is 5 mm (0.20 inches) deep is completely ignored in these analyses. What was found was that there were relatively short growth times until the crack grows through the thickness. However, in addition to the two sources of uncertainty already mentioned, there are some serious reservations about the stress-corrosion cracking growth model. The discussion sections will overview alternative ways to estimate the PWSCC crack growth law and the corresponding constants based on observed field crack growth data. However, it is what was available, so it was used.

Figure G.52 (a-c) provides the results of these calculations. The axial cracks were introduced into the center of the weld. As discussed previously, there are numerous crack initiation sites provided by the grinding process of which any could begin to grow. In reality, the grinding scratch near the region of highest residual stress is expected to be the preferred dominant crack initiation site. Identification of the different plots is made as follows. In the legend above the plots, the curves are labeled as '3.0 Residual I-O' for instance (Figure G.52 (a)). This represents the crack shape after 3.0 months of PWSCC with residual stresses only and welding from the inside first followed by completing the outside welds. The label '3.0 Load I-O' indicates the 3 month PWSCC crack shape for the case where the operating loads are applied overtop the residual stress field (nonlinear analysis) for the I-O weld case.

The first thing of note is that the growth of the crack in the residual stress field without any applied loading is lower than when the load is applied. The plot shows the normalized (by the pipe thickness) crack depth. At the end of two years, with only the residual stresses, the crack is about 20 percent through the thickness. When the operating load is applied, the crack is 95 percent through the thickness after one year. At about 14 months the crack becomes a through wall crack (TWC).

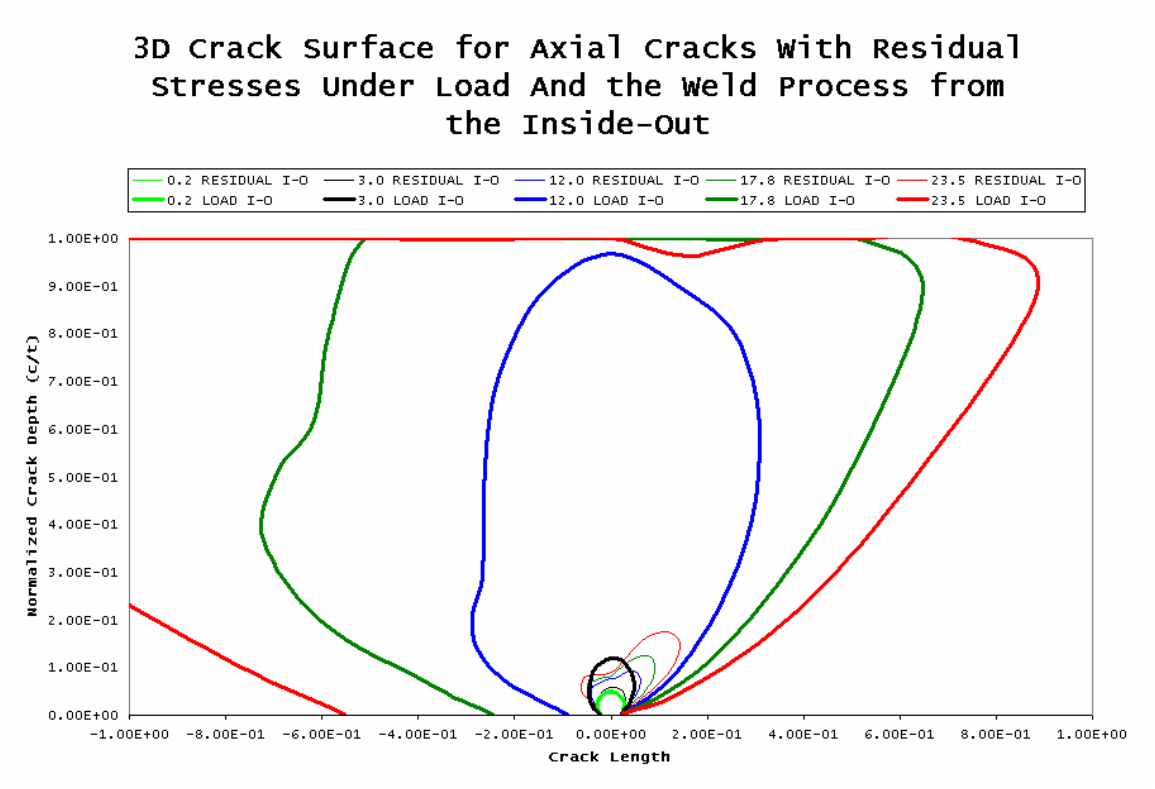

Figure G.52(a) Axial crack growth for the inside-out weld process

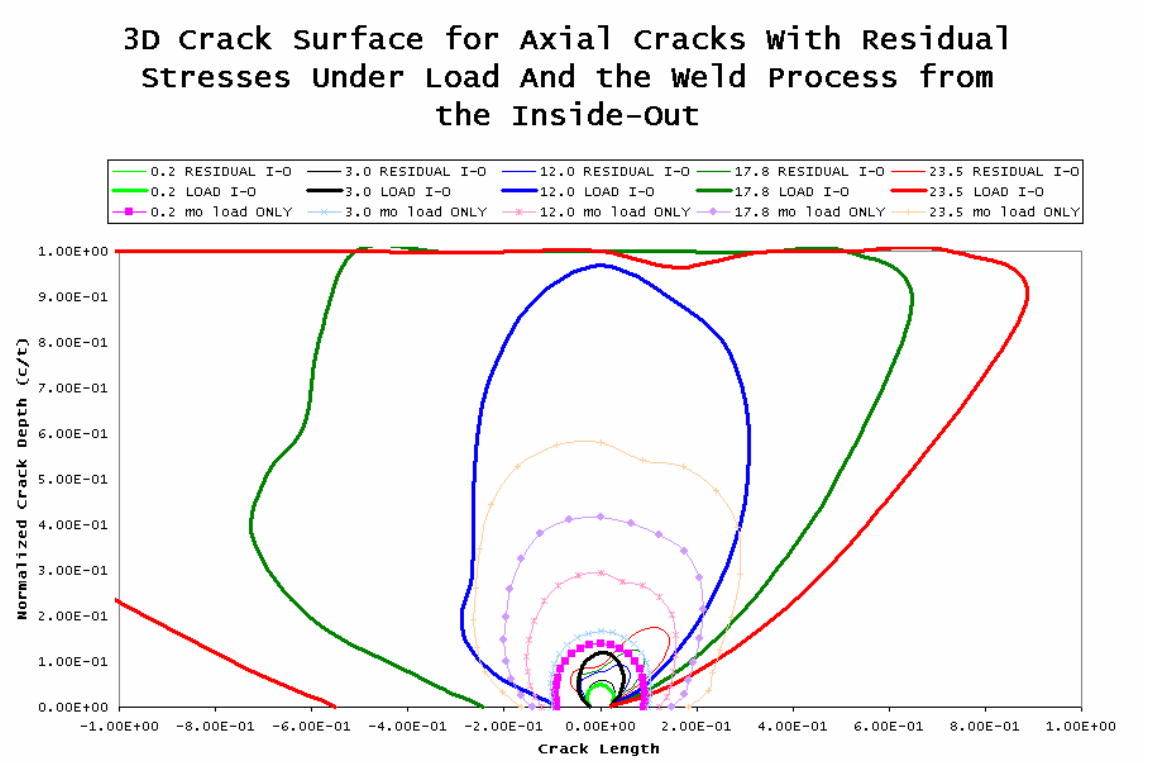

Figure G.52b Approximation for the impact of the residual stress field on the crack size and shape

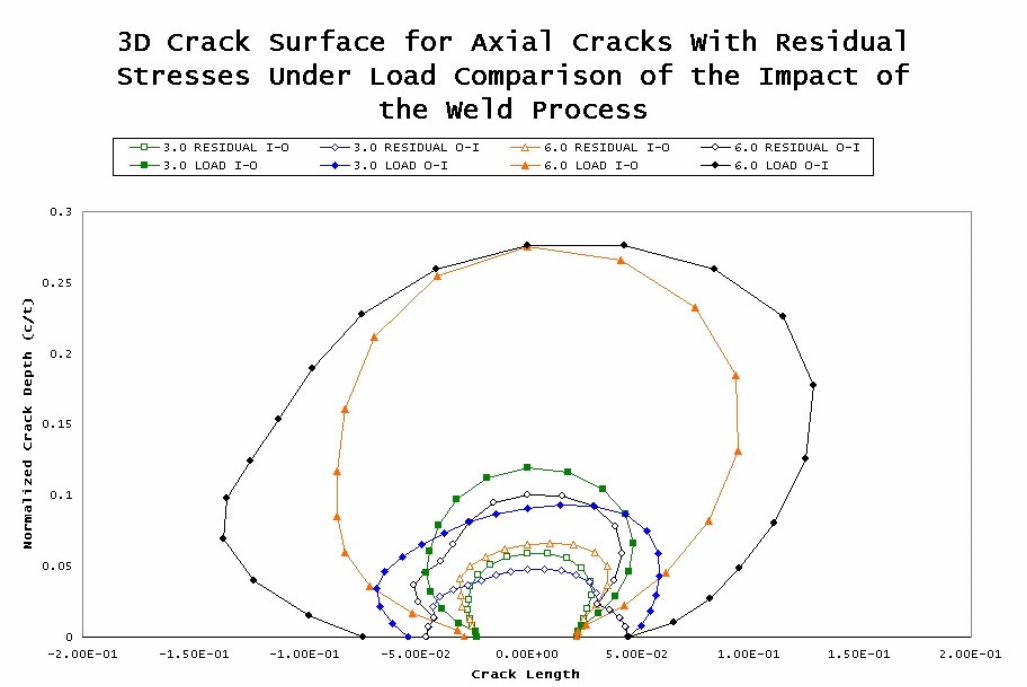

Figure G.52c Three and six month crack growth shapes

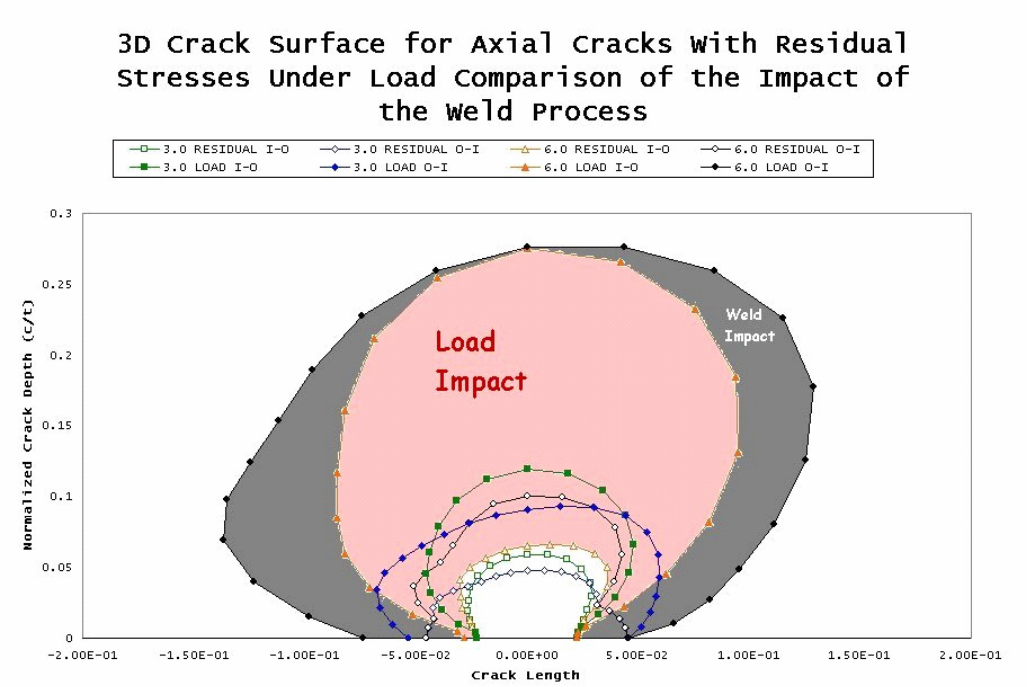

Figure G.53 Approximation for the impact of the residual stress field on the crack size and shape. The 'red' shape represents the crack shape for the case of loading and residual stresses (for the I-O case) and the 'white' shape is the crack shape for the residual stress only case after 6 months of PWSCC growth. The 'red' curve (I-O case) can be compared to the 'gray' (O-I case) curve for a comparison of the weld sequence effect

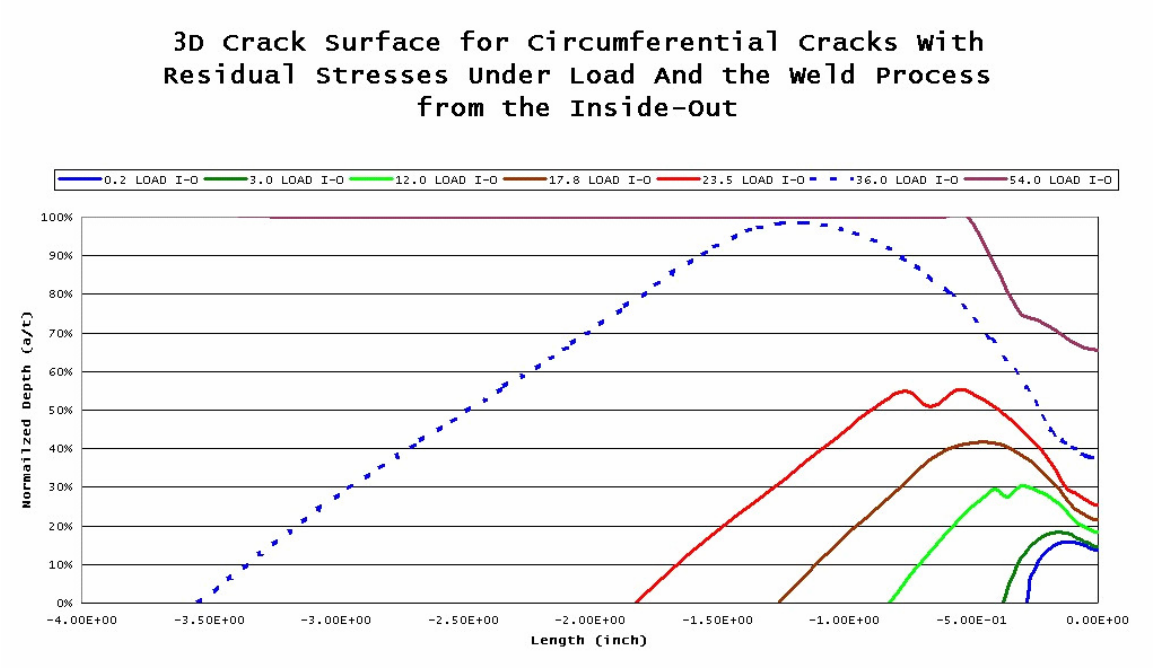

Figure G.54(a) Circumferential PWSCC growth – inside weld first case

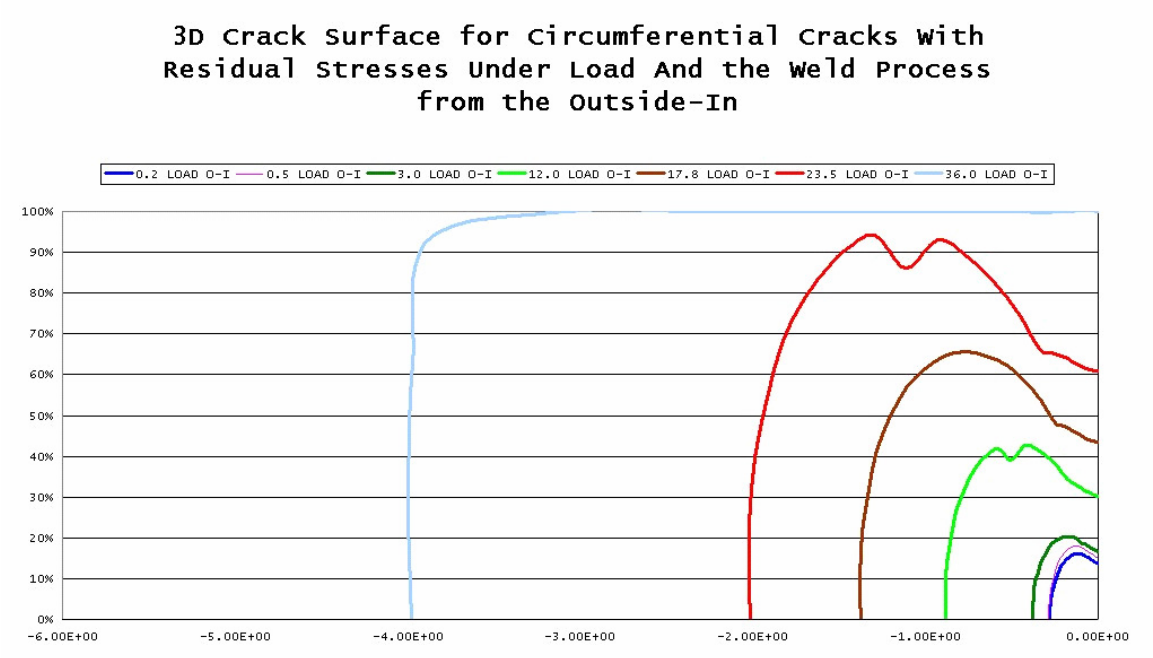

Figure G.54b Circumferential PWSCC growth – outside weld first case

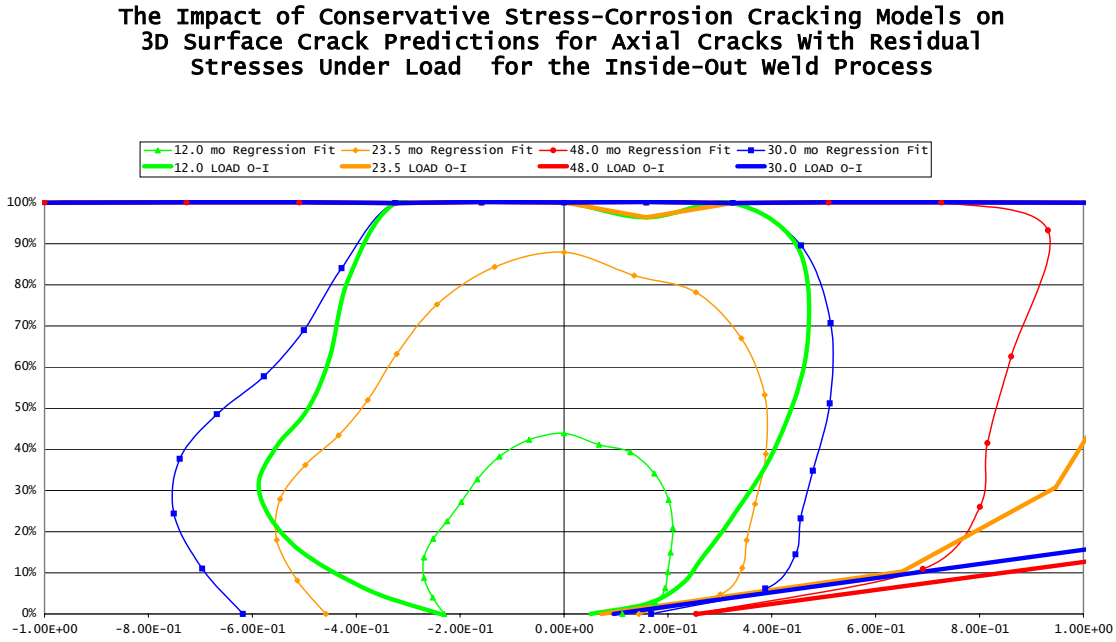

Figure G.55(a) The impact of using a conservative PWSCC law on crack growth – axial crack

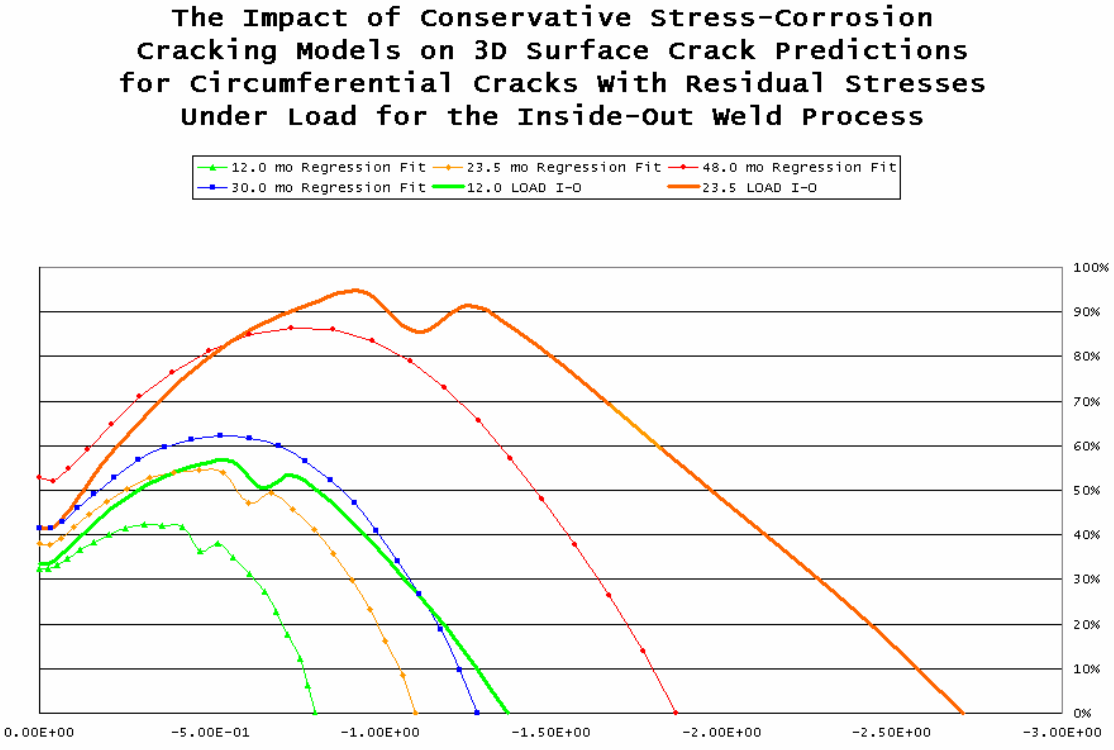

Figure G.55b The impact of using a conservative PWSCC law on crack growth – circumferential crack

The small growth due solely to the residual stresses may seem like these residual stresses have little impact on PWSCC. However, if we perform an approximate analysis and assume that superposition applies in determining the stress intensity factors to use in the PWSCC equation, then we can estimate the impact of the residual stress field. For this we subtracted the stress intensity factors for the residual stress fields only from the residual stress fields with the operating loads applied. (Recall that the loads were applied on top of the residual stress fields and all history, including plastic strains were accounted for.) Figure G.52 (b) shows this calculation for a number of different times. As an example, after 12 months, the 'dark blue' curve represents the crack shape for the I-O weld for the case of residual stress and applied service loads. It is seen that the crack is approximately 95 percent through the pipe wall. The pink curve labeled '12 mo load only' represents the crack shape for a load only case after 12 months of PWSCC, i.e., no residual stresses are included. This crack is about 32 percent through the pipe wall. The small light blue curve represents the crack shape for residual stress only after 12 months. This crack is only about 12 percent through the pipe wall. Hence, because the crack growth law is a nonlinear function of stress intensity factor, and additional plasticity occurs as the service loads are applied over top the weld residual stresses, the effect of the residual stresses on PWSCC is significant.

Finally, Figure G.52 (c) shows the three and six month crack growth shapes for both the inside first weld followed by the outside weld (I-O) and the outside weld first, then inside weld (O-I) case. One can also compare the crack shape and depth for the residual stress only case and the residual stress plus load cases.

In Figure G.53 is identical to Figure G.52 (c) except shading is introduced to point out these effects. The 'red' shape represents the crack shape for the case of loading and residual stresses (for the I-O case) and the 'white' shape is the crack shape for the residual stress only case after 6 months of PWSCC growth. The 'red' curve (I-O case) can be compared to the 'gray' (O-I case) curve for a comparison of the weld sequence effect.

Figure G.54 shows the circumferential crack growth shape after three and six months for the different cases. The O-I case tends to grow cracks wider than the corresponding I-O case while for the I-O case, the cracks grow somewhat deeper. This is expected by comparing the hoop residual stresses between the two analysis cases (Figures G.43, G.44, G.48 and G.50).

Equation (G.1), which was taken from Reference G.13, was a fit to the available test data (Figure 4-2 in Reference G.13). The fit of the data was conservative and tends to represent an upper bound to the PWSCC crack growth predictions. If that same data is taken and a least squares regression fit to the data provided, the following is obtained:

$$\frac{da}{dt} = 2.16 \times 10^{-11} (K_I - 9)^{0.8} (m/\sec) \qquad \text{(G.2)}$$

Comparing Equations G.1 and G.2, one notices that the constant is larger and the exponent is smaller in Equation G.2. A comparison of the predicted PWSCC crack growth using the less conservative regression fit (Equation G.2) to the original law is shown in Figure G.55.
Figure G.55 (a) illustrates that an axial crack will break through the pipe wall sometime after 2 years using the regression fit compared to about 1 year using the conservative PWSCC rate curve. In Figure G.55 (a) and G.55 (b), the label '12.0 mo Regression Fit' represents the crack shape after 12 months of PWSCC growth using the Equation G.2 regression fit while '12.0 Load O-I' is the crack shape using Equation G.1. Similar notation is used for other times, i.e., '23.5 Load O-I' represents the PWSCC crack shape after 23.5 months using Equation G.1, etc. Figure G.55 (b) indicates that the circumferential crack will break through the pipe wall after 4 years using the regression PWSCC rate curve compared with about two years using the conservative PWSCC rate equation. This illustrates the importance of using a correct PWSCC law and the need for more PWSCC data. Moreover, from Figure 4-2 in

Reference G.13, it is clear that significant scatter exists in the PWSCC test data. Because of this scatter, a risk based probabilistic assessment of PWSCC is in order.

G.7.2 The 3 Dimensional Growth of Circumferential Cracks Through the Hot Leg/RPV Nozzle Bimetal Weld

Axial crack growth in the hot leg/RPV nozzle bimetal weld is mainly driven by the hoop stresses, although stress redistribution during PWSCC crack growth through the pipe wall thickness is influenced slightly by other stress components. Figures G.48 and G.50 show the contour plots of hoop stresses (i) after welding and heating to 324°C (615°F) and (ii) service loads applied to the (i) case.

Circumferential crack growth is mainly driven by the axial stresses. Referring to Figure G.38, note that the tensile axial stresses at room temperature are nearly all reversed to compression in the weld region as the pipe system is heated to 324°C (615°F). The end conditions of the hot leg (reactor vessel and stream generator) are assumed fixed for the thermal analysis. As such, when the hot leg is heated up, it is constrained from expansion at the ends. The residual stresses reduce to compression as seen in Figure G.38. In contrast, the axial expansion of the hot leg has minimal effect on hoop stresses.

Referring to Figures G.38, G.47 and G.49, compressive axial stresses exist in the pipe near the weld region for the case of no load except in a small region on the inside surface near the buttering region. Hence, circumferential crack growth *due solely to residual stresses (at 324°C (615°F) operating temperature)* is not expected except for possible small growth at the inside surface near the butter region. The bottom illustrations in Figures G.47 and G.49 represent axial stresses with the loads (pressure, tension, and bending – see Figure G.46) applied. The loads were applied to the initial conditions of residual stress state at 324°C (615°F). Very little additional plasticity occurred during application of the loads because the axial residual stress state is compressive before application of the load. For the hoop load case, because the initial hoop residual stresses are high before application of the load, plasticity during application of the pressure does occur. From Figures G.47 and G.49, it is clear that the applied loads would be the main contributor to circumferential crack growth in contrast to axial crack growth where the hoop residual stresses dominate crack growth.

The circumferential crack growth profiles for the I-O and O-I cases are shown in Figures G.54a and G.54b. The initial flaw size for this case is 5 mm (0.2 inch) also. Because the 3D model has a symmetry plane at the center of the elliptic cracks, only the crack shape from 0 to 90-degrees is shown. It is seen that crack growth favors a location at an angle away from the deepest point of the crack. This is somewhat typical for circumferential cracks in homogeneous materials (Ref. G.14). It takes approximately 3 years for the crack to break through the pipe wall. The axial cracks grow about twice as fast.

The crack growth law shown in the above equation was obtained from (Ref. G.13) and was necessarily conservative. If a regression fit is made of the PWSCC test data for Alloy 182 at 324°C (615°F) (Figure 4-2 of Reference G.13), different growth response is obtained. Figure G.55a and G.55b compare axial and circumferential crack growth for different PWSCC growth laws. It is clearly seen that crack growth predictions depend strongly on the accuracy of the SCC data fit. The SCC predictions would be best interpreted using a probabilistic approach using TRACLIFE.

G.8 THREE DIMENSIONAL WELD EFFECTS

As discussed in References G.1, G.11, and G.13, the bimetallic hot leg weld that experienced field cracking had a number of repairs done to it. Because repair welds are inherently three dimensional in nature, some limited analyses were performed in order to obtain a qualitative assessment of three-dimensional effects on the bimetallic weld and weld repair process.

Figure G.56 illustrates the model that was considered. The butter layer, PWHT, and hydro-test were not considered, and the boundary conditions at the vessel and steam generator were not considered (i.e., the length of pipe shown in Figure G.56 was modeled). All of the weld passes shown in Figure G.20 were not considered. Rather, passes were lumped together to form 7 passes as shown in Figure G.56. All of the conditions in Figure G.23 could well have been considered, but were neglected due to time constraints. In the future, it may be useful to perform complete 3D analyses of this pipe.

Figure G.57 illustrates the repair cases considered: two different lengths and two different depths. All four analyses considered the baseline weld first followed by grinding and deposition of the repair weld passes. The definitions of the original weld and repair weld geometry convention are shown in Figure G.58. The X = 0 location represented the start/stop positions of the baseline weld. The repair welds modeled ranged from A to B (Length L_2) and A to C (Length L_1) with the angular definitions shown in Figure G.58. Figure G.59 shows the analysis on the long (L_1) and deep (d_2) weld repair in progress.

Axial residual stresses for the baseline three-dimensional weld are shown in Figure G.60. The section is at the center of the weld and includes the A508 nozzle. Notice that the axial stresses near the start location are different from a location far away from the start location where near steady state conditions exist. In essence, the axial stresses reverse sign compared with locations away from the start/stop location. This can actually help in slowing down circumferential SCC growth as the crack grows into this location. Figure G.61 shows a similar axial stress plot for the baseline weld for a longitudinal cut section. Figure G.62 shows a similar plot of the Z-component stresses (see coordinate axis in Figure G.62). It is also seen that compressive stresses develop near the start/stop location that can slow down longitudinal crack growth. However, this reduction in residual stress state must be balanced by the fact that start/stop locations are often regions where weld defects can occur. Note that the Z-component stresses represent hoop stresses on the cut planes.

Figure G.63 compares weld residual stresses between the axis-symmetric and three-dimensional analyses at room temperature. Of course, the three-dimensional solution did not include the butter step, the PWHT after buttering, and the passes were deposited in only seven passes. Despite these differences, the comparison of hoop stresses at a location far from the start/stop location is not entirely dissimilar. In general, the three dimensional solution predicts more compression in the weld at the inside surface compared with the axis-symmetric solution.

Figure G.64 shows weld residual stresses after repair weld case 1 is complete. This is the case of the long, shallow weld repair (see definitions in Figure G.58). Axial residual stresses reverse sign near the start and stop locations of the repair while stresses within the middle of the repair do not change much from the baseline steady state locations. Figure G.65 shows a similar plot of axial stresses for a segment that consists of an angular cut of the weld repair. The effect of the repair on residual stresses is evident. Figures G.66 and G.67 show similar results for the repair case for the short, shallow weld repair. Figure G.67 is a plot of mean stress, which is a measure of constraint caused by welding and repair. It is seen that the weld repair does induce significant constraint near the beginning and end points of the repair. Constraint can influence fracture response, and possibly SCC rates, but were not considered here since little work has been performed to date that investigates the effect of constraint on SCC rates.

Figures G.68 and G.69 show axial and mean stress for the short, deep weld repair. Comparing Figures G.66 and G.67 to Figures G.68 and G.69 shows that the compressive stress that develops near the beginning and end of the weld repairs is deeper for the deeper repair. This actually suggests that weld repairs may help slow down SCC growth and act as crack stoppers. Figure G.70 provides a plot of

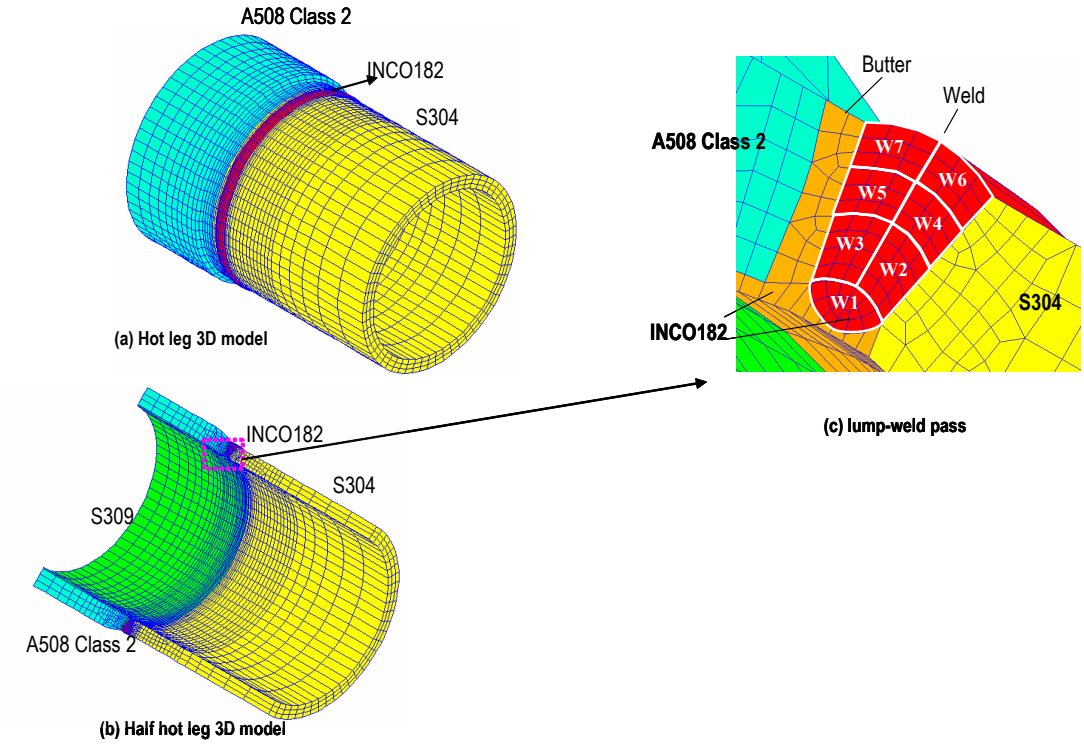

Figure G.56 Hot leg 3D analysis geometry

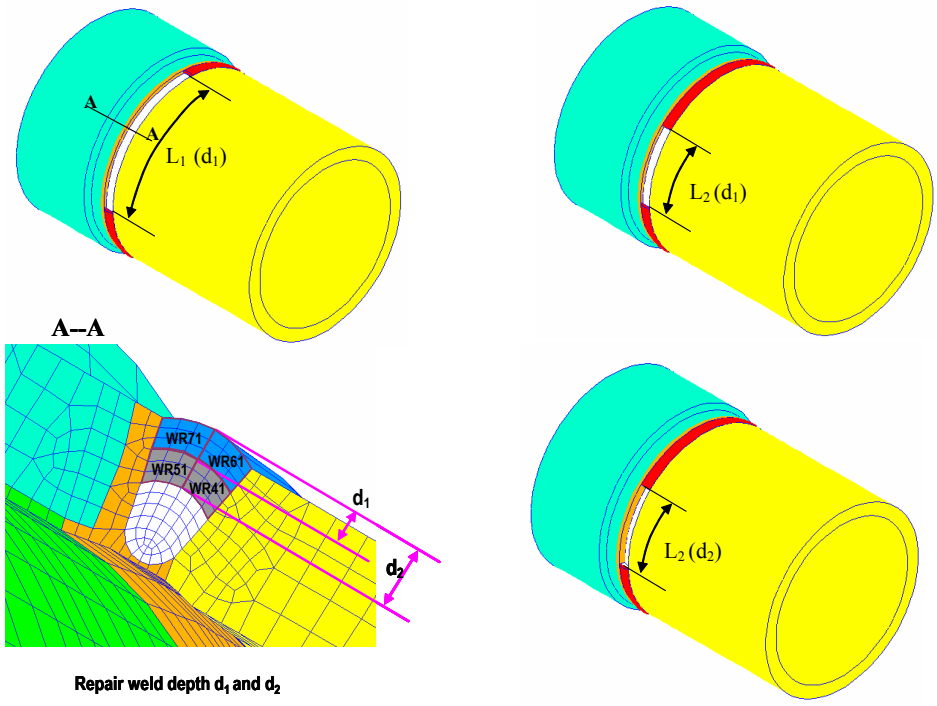

Figure G.57 Two-length and two-depth repair analyses

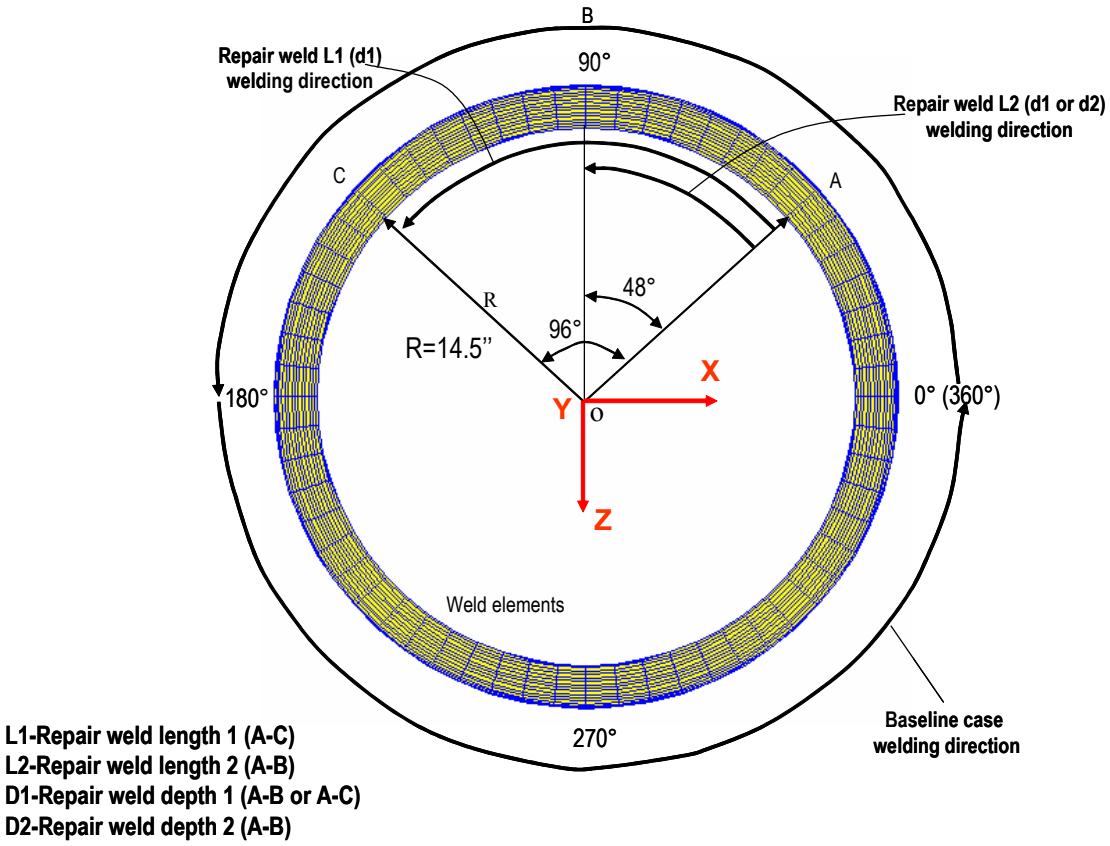

Figure G.58 Weld directions

Ground out

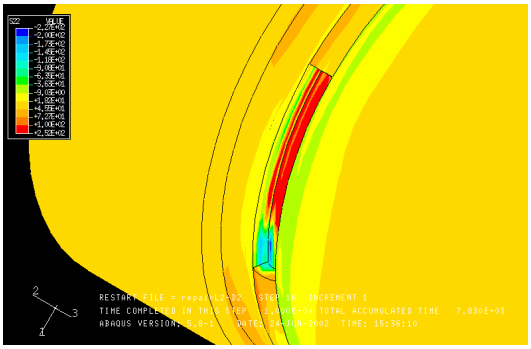

After repair

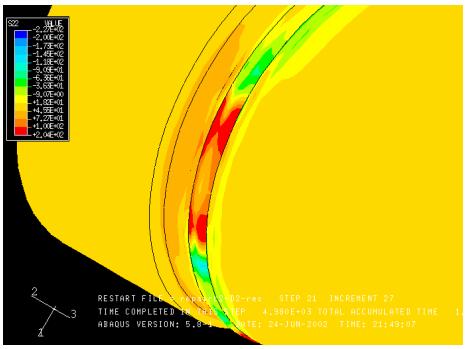

Repair length
L2-D2

Figure G.59 An example of the grinding and weld repair model during analysis

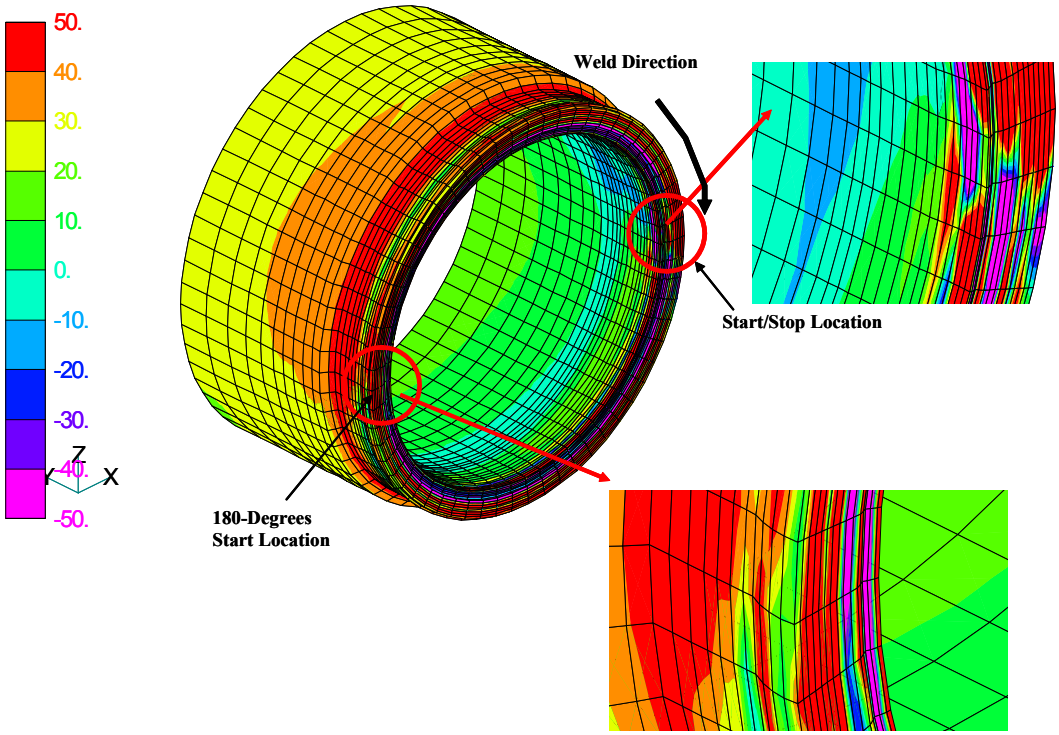

Figure G.60 Baseline weld – axial stresses

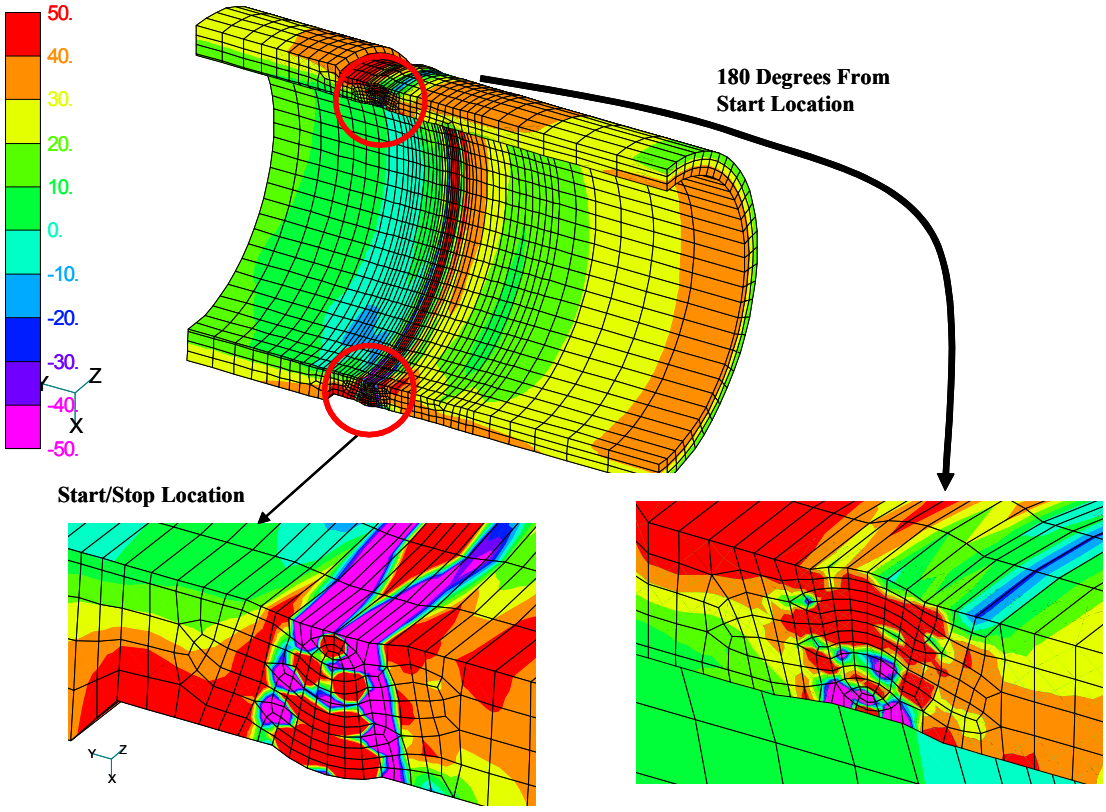

Figure G.61 Baseline weld – axial stresses

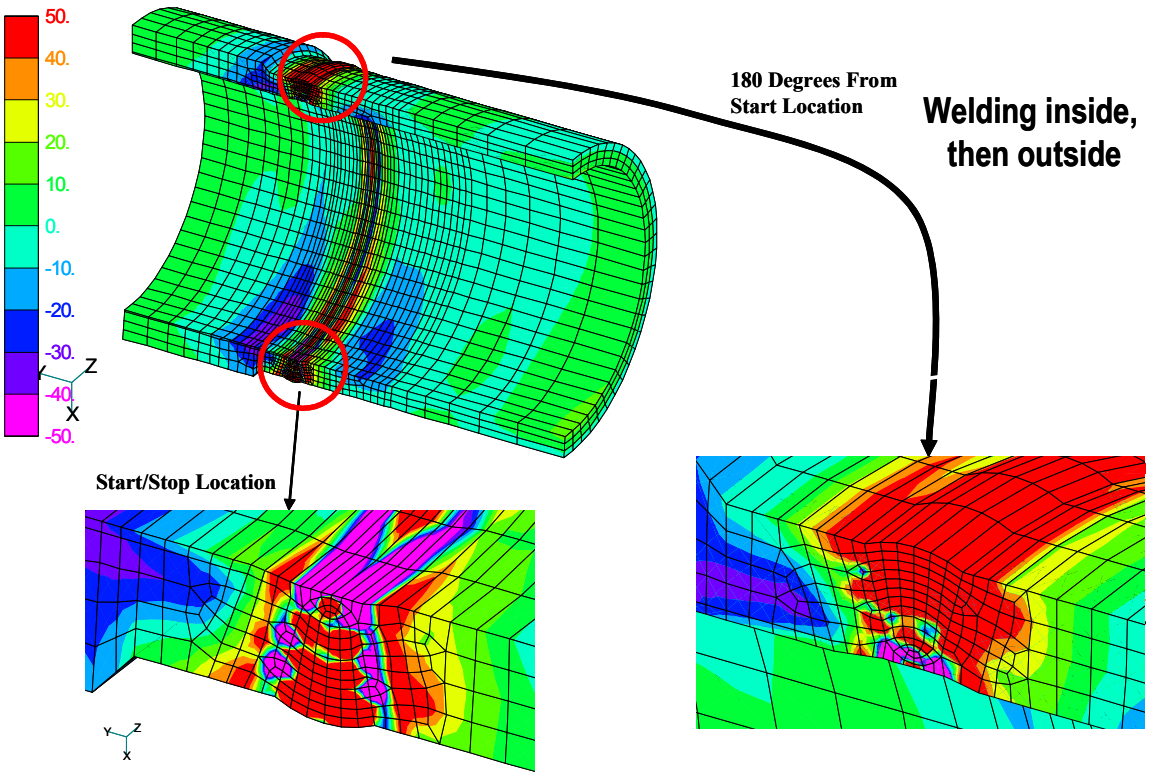

Figure G.62 Baseline weld – Z-component stresses (these represent hoop stresses on the cut planes)

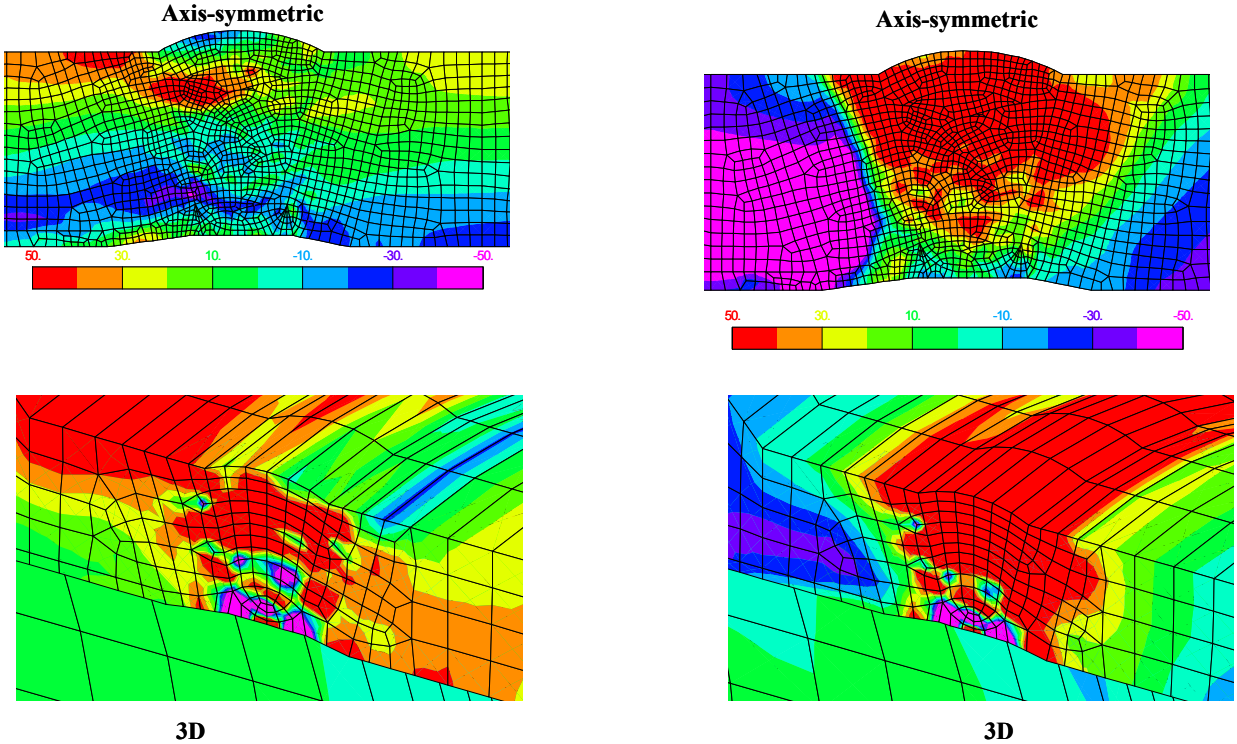

Figure G.63 Comparison of axial and hoop stresses between the axis-symmetric and 3D solutions

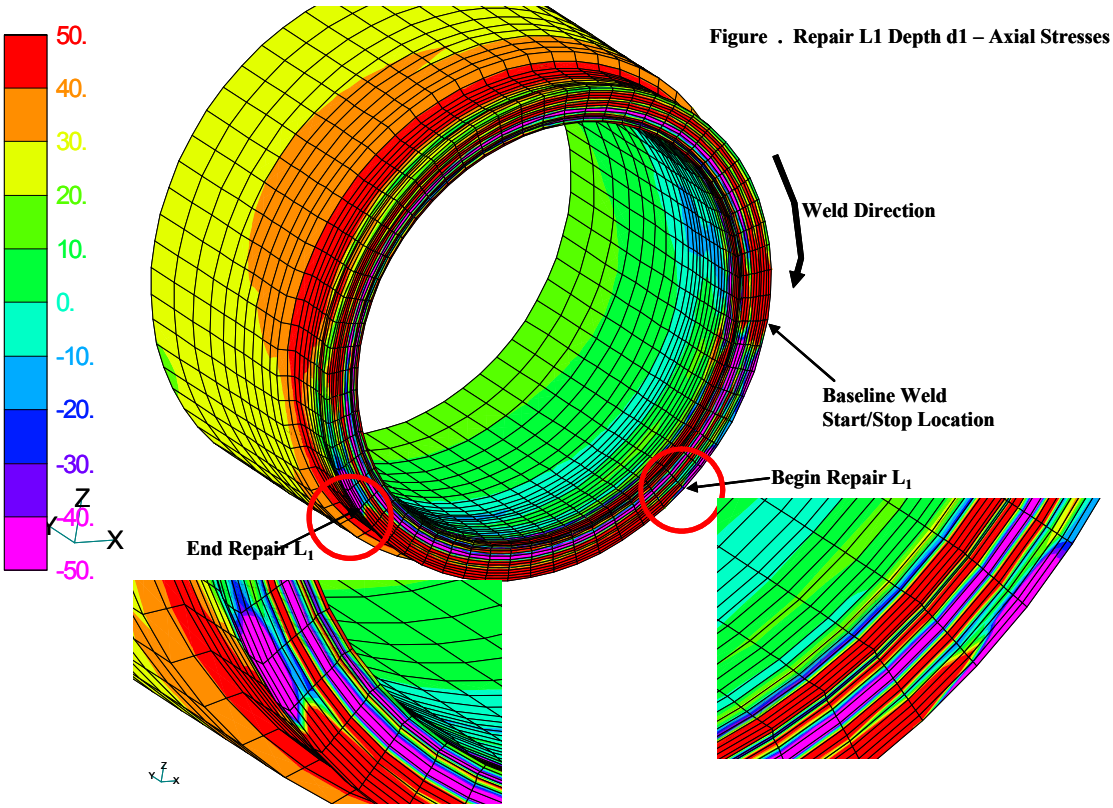

Figure G.64 Comparison of axial stresses for repair case number 1

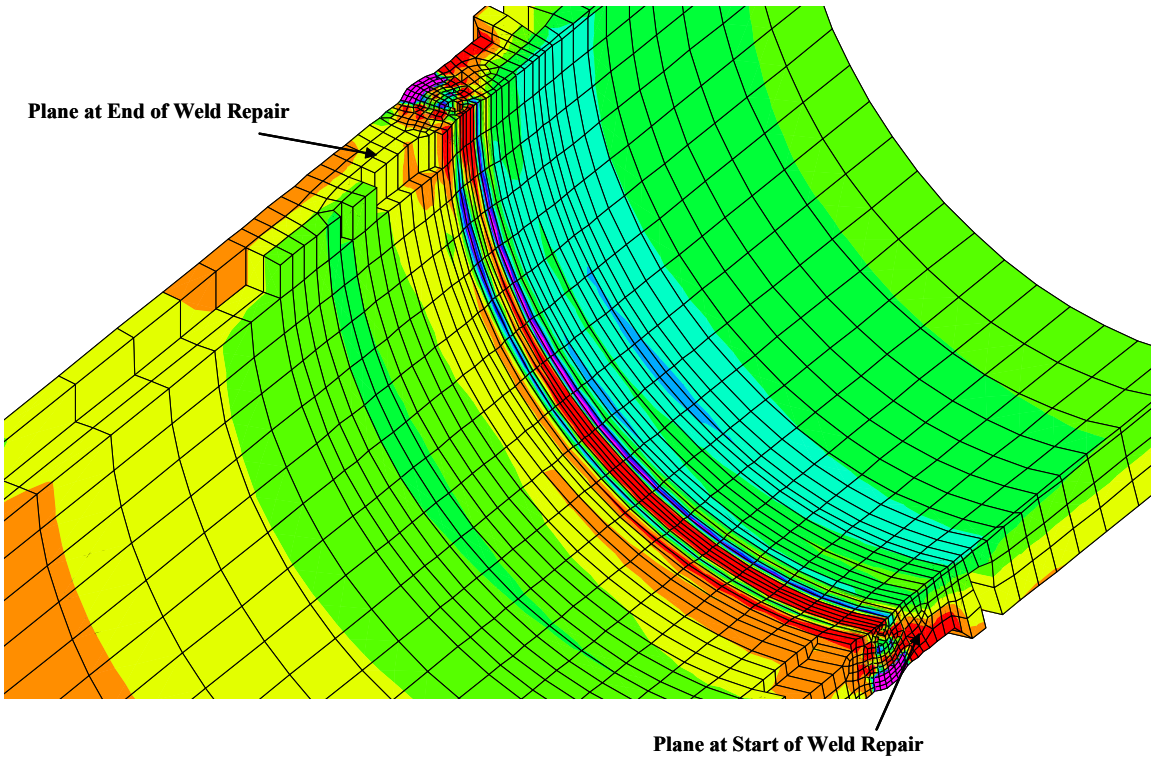

Figure G.65 Comparison of axial stresses for repair case number 1

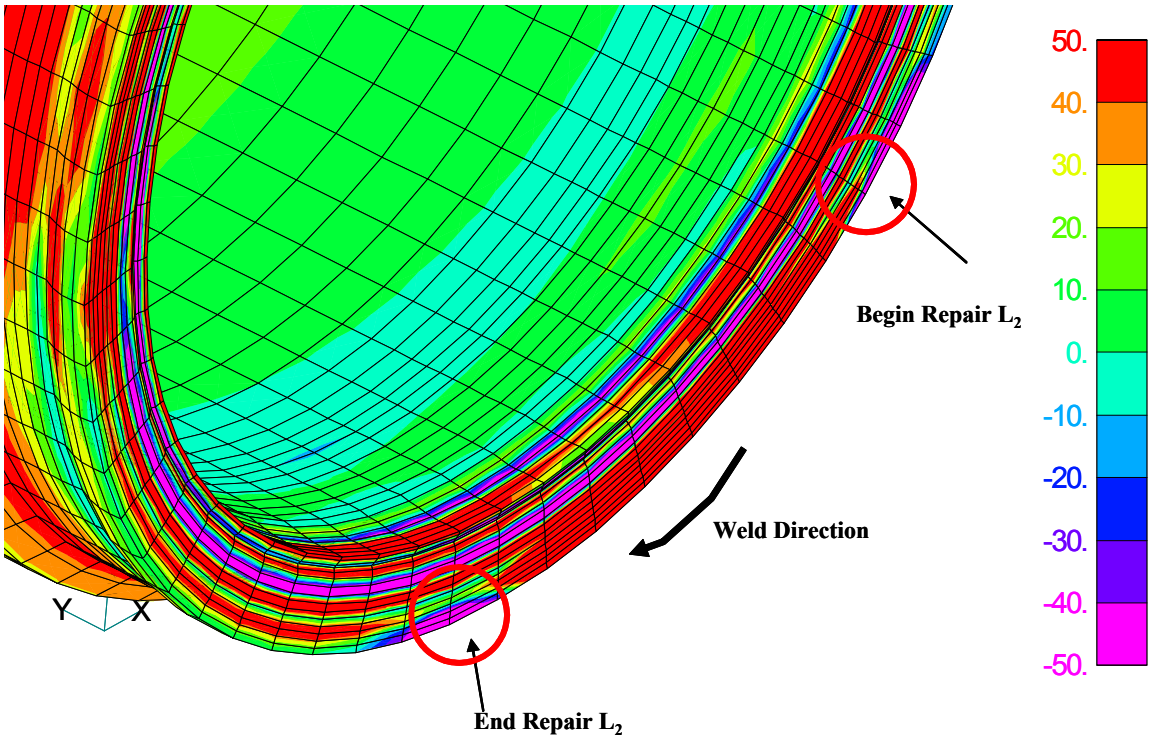

Figure G.66 Repair L2 depth d1 – axial stresses

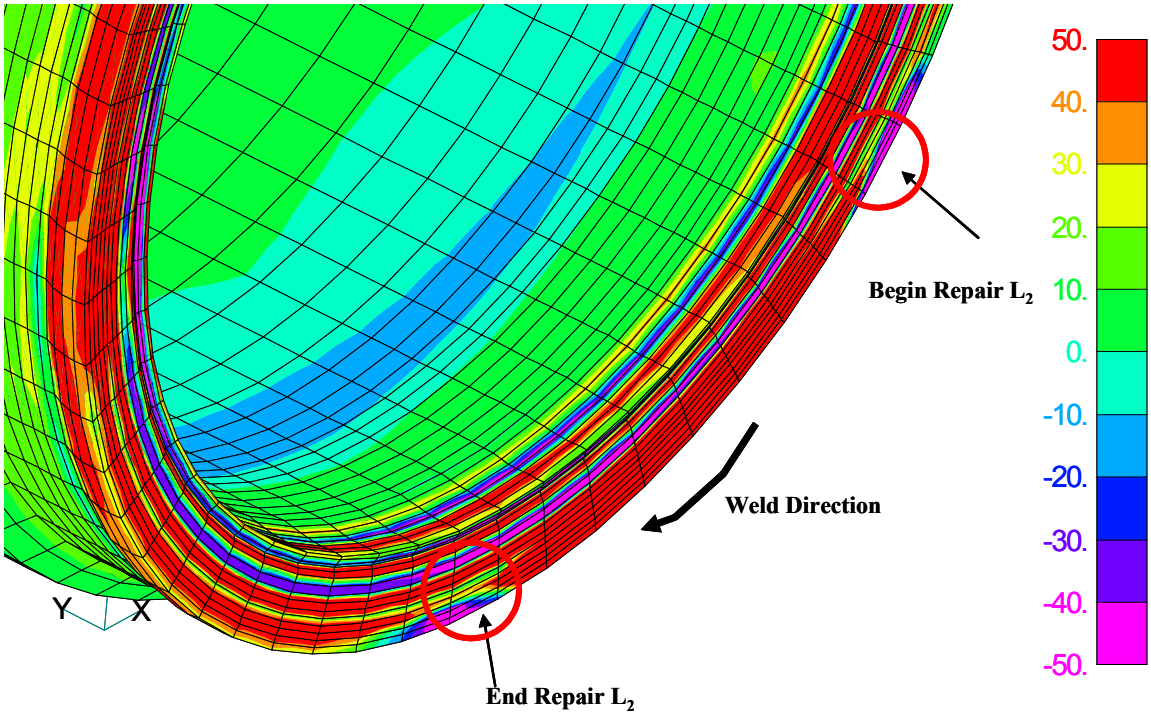

Figure G.67 Repair L2 depth d1 – mean stress ($\sigma_{kk}/3$)

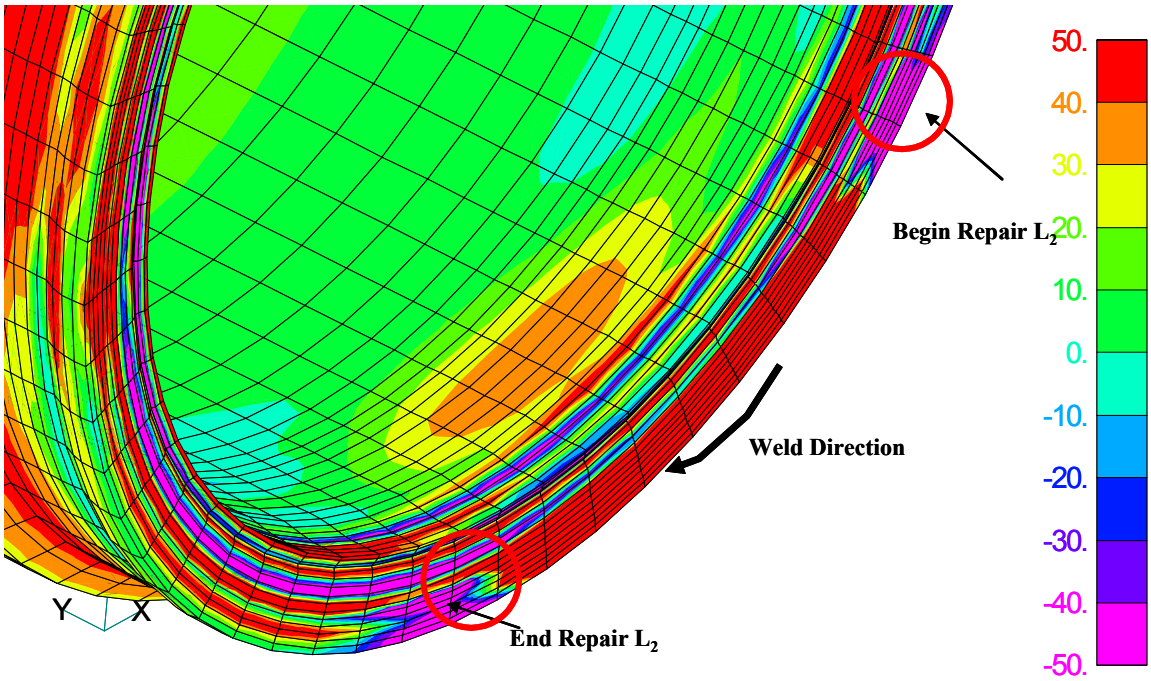

Figure G.68 Repair L2 depth d1 – axial stresses

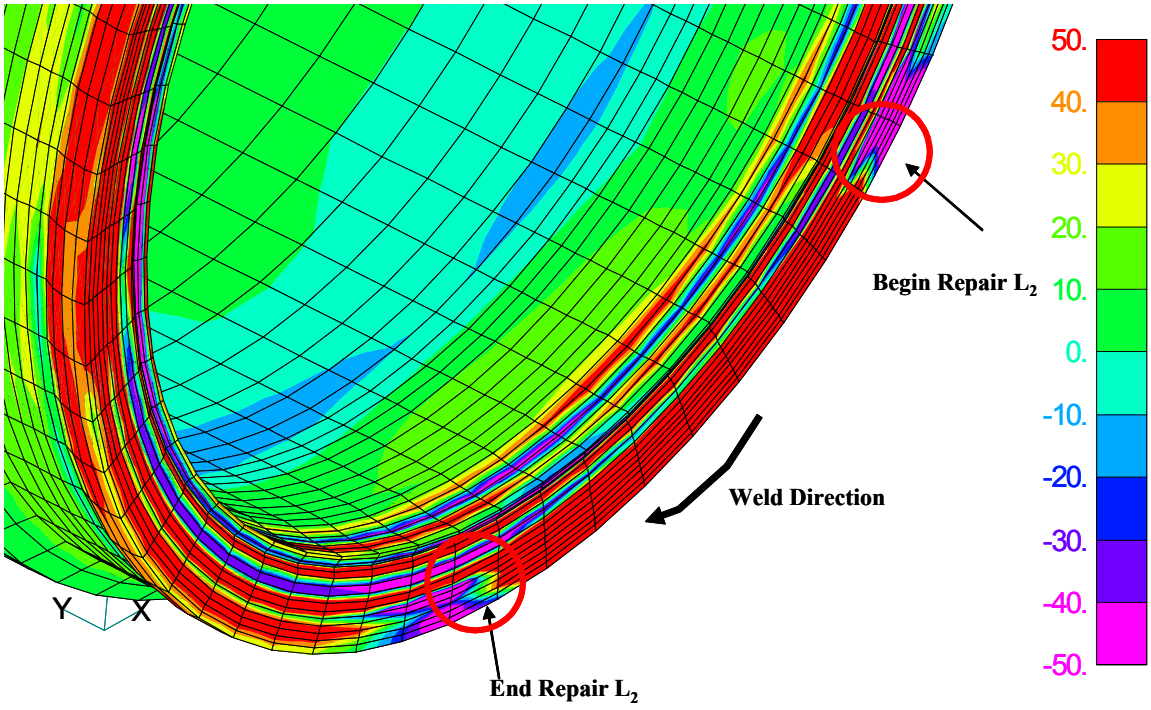

Figure G.69 Repair L2 depth D2 – mean stress ($\sigma_{kk}/3$)

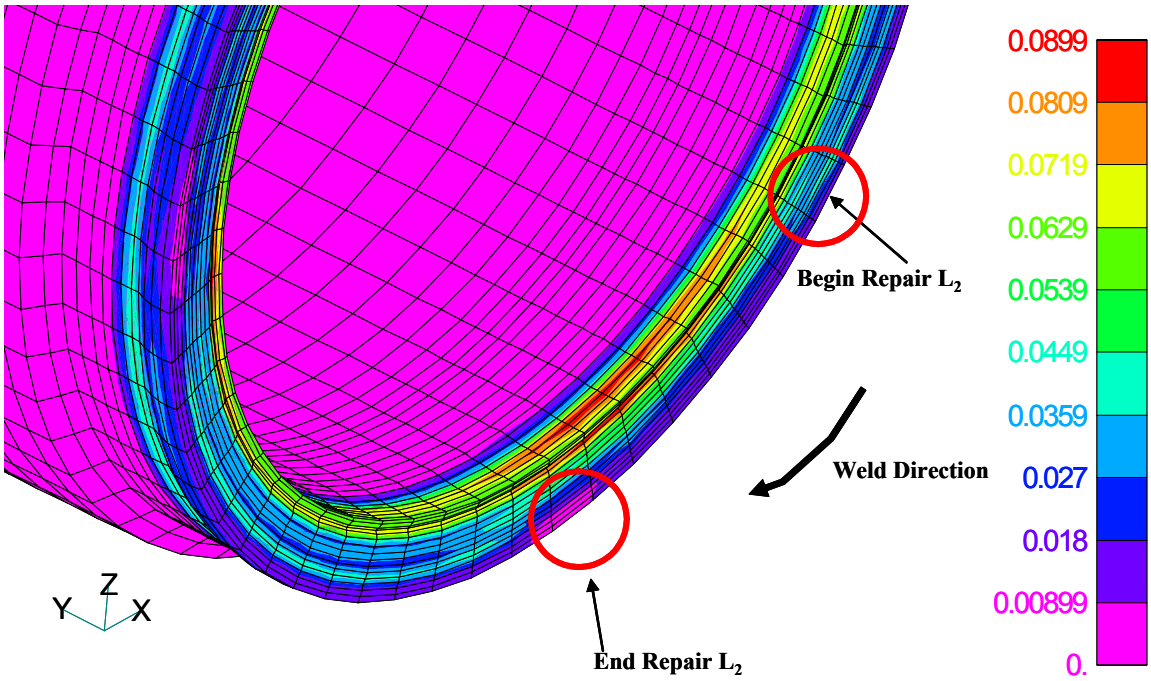

Figure G.70 Repair L2 depth d2 – equivalent plastic strain

equivalent plastic strain for the short, deep repair. It is clear that plastic strains increase along the entire length of the repair.

G.9 DISCUSSION AND CONCLUSIONS

Analyses of the residual stresses and PWSCC for the hot leg/RPV nozzle bimetal weld of the V. C. Summer plant were performed. The entire history of fabrication of the weld was included in the analysis, including Inconel buttering, PWHT, weld deposition, weld grind-out and repair, hydro-testing, service temperature heat-up, and finally service loads. Some of the conclusions are described in the bullets below.

- An analysis of a cold leg pipe bimetal weld was performed first and residual stresses were measured from a bimetallic weld section that Battelle had secured earlier from a canceled plant. The measurements appeared rather low compared with what was expected. For instance, hoop stresses in the weld were compressive at both the inside and outside surfaces of the pipe. This does not appear reasonable based on experience. As such, additional measurements of bimetallic pipe welds should be made using a different measurement technique.

- To obtain a reasonable description of fabrication induced residual stresses, all of the fabrication steps should be considered in the analyses.

- The as fabricated axial weld residual stresses alternate sign as one proceeds from the inside to the outside surface of the pipe near the weld region. Tension to compression to tension back to compression axial residual stresses develop in the as fabricated pipe weld. The tensile stresses were highest at the inside surface for the case of the outside weld repair deposited first and finishing with the inside weld compared with the opposite case.

- For reducing the effect of circumferential PWSCC after weld repairs, inside welding followed by outside welding is preferred.

- Final hoop residual stresses after complete fabrication are mostly tensile in the weld region. For the case of outside welding

followed by inside welding after the bridge repair, high tensile residual stresses are produced everywhere. For the inside weld followed by outside weld case, a small zone of compressive hoop residual stresses develop at the pipe ID in the weld.

- Hydro testing does not alter fabrication residual stresses very much.

- Heating the hot leg pipe system up to operating temperature of 324°C (615°F) reduces axial fabrication stresses to mainly compressive values due to the rigid constraint provided by the vessel and steam generator. Hoop residual stresses are unaffected by heating up to operating temperatures.

- Since as fabricated axial residual stresses are low at operating temperature, circumferential stress corrosion cracking is not expected due solely to fabrication stresses. Service loads dominate circumferential SCC.

- Axial crack growth is dominated by fabrication residual stresses.

- Weld repairs can alter residual stresses in pipe fabrications. In general, stress reversal in sign occurs near the start/stop locations of the repair. This can possibly result in a SCC crack stopper or slow down the crack growth. A similar reversal in the sign of the stress occurs in a baseline weld near the torch start/stop locations.

- Based on the PWSCC crack growth law from Reference G.13 and the analysis results here, axial cracking should be confined to the weld region. Starting from a crack 5 mm (0.2 inches) in depth, the crack should break through the pipe wall within two years. The crack nucleation time is something that should be studied in more detail.

- Circumferential cracks should take about twice as long to become a through wall crack compared with axial cracks. Circumferential cracks will tend to grow longer than axial cracks. However, since service loads dominate circumferential cracks, they will slow their circumferential growth as they grow toward the bottom of the pipe. Here, by bottom of the pipe, it is understood to be the compressive bending stress region of the pipe. The service loads consist of thermal expansion mismatch, tension caused by 'end cap' pressure, and bending. The bending stresses caused by a bending moment are compressive 180 degrees from tension zone. Part through circumferential cracks that initiate in the tension zone and grow beyond the bending neutral axis may slow down as they approach the compressive bending stress zone. However, for non-fixed bending axes, where the tension zone changes, this may not be significant.

- PWSCC growth would be best considered using a risk based probabilistic approach using TRACLIFE.

- Weld repairs alter pipe residual stress fields near the start/stop regions of the repairs. This may help slow down a growing stress corrosion crack.

- Grinding of welds may lead to scratches, which in turn may lead to crack initiation sites. Grinding of welds should be performed carefully. It is of use to study the effect of grinding on both residual stresses (caused by grinding) and crack initiation sites. Numerical models of the grinding process can be developed.

G.10 REFERENCES

G.1 McIlre, A. R., "PWR Materials Reliability Project Interim Alloy 600 Safety Assessments for US PWR Plants (MRP-44) – Part 1: Alloy 82/182 Pipe Butt Welds", EPRI Report, TP-1—1491, April, 2001.

G.2 Scott, P. M., et al., "Fracture Evaluations of Fusion Line Cracks in Nuclear Pipe Bimetallic Welds", NUREG/CR-6297, January, 1995.

G.3 VFT™ (Virtual Fabrication Technology Software), Version 1.3, Developed Jointly by Battelle and Caterpillar (Caterpillar owned),

exclusively distributed by Battelle Columbus Ohio, and The Welding Institute (TWI) (via separate contract with Battelle), Cambridge, England.

G.4 FRAC@ALT© (FRacture Analysis Code via ALTernating method), Version 2.0, January, 1999, Battelle Memorial Institute.

G.5 TRACLIFE™, Probabilistic Life Prediction Code, R. E. Kurth, Battelle, 2001.

G.6 Brust, F. W., Stonesifer, R., Effects of Weld Parameters on Residual Stresses in BWR Piping Systems EPRI NP-1743, Project 1174-1, 1981.

G.7 Brust, F.W., Dong, P., and Zhang, J., 1997, "A Constitutive Model for Welding Process Simulation Using Finite Element Methods," Advances in Computational Engineering Science, Atluri, S.N., and Yagawa, G., eds., pp. 51-56.

G.8 F. W. Brust and M. F. Kanninen, "Analysis of Residual Stresses in Girth Welded Type 304-Stainless Pipes", ASME Journal of Materials in Energy Systems, Vol. 3, No. 3, 1981.

G.9 Dong, P., and Brust, F. W. "Welding Residual Stresses and Effects on Fracture in Pressure Vessel and Piping Components: A Millennium Review and Beyond", Transactions of ASME, Journal Of Pressure Vessel Technology, Volume 122, No. 3, August 2000, pp. 329-339.

G.10 Thomas, A., Ehrlich, R., Kingston, E., and Smith, D. J., "Measurement of Residual Stresses in Steel Nozzle Intersections Containing Repair Welds", in ASME PVP Volume PVP 434, Computational Weld Mechanics, Constraint, and Weld Fracture, Edited by F. W. Brust, August, 2002.

G.11 Schmertz, J. C., Swamy, S. A., and Lee, Y. S., "Technical Justification For Eliminating Large Primare Loop Pipe Rupture As the Structural Design Basis for the Virgil C. Summer Nuclear Power Plant", Westinghouse Report, WCAP-13206, April, 1992.

G.12 Rao, G. V., et al., "Metallurgical Investigation of Cracking in the Reactor Vessel Alpha Loop Hot Leg Nozzle to Pipe at the V. C. Summer Nuclear Generating Station", WCAP-15616, Westinghouse Electric Company, January 2001.

G.13 Westinghouse Electric Co., "Integrity Evaluation for Future Operation Virgil C. Summer Nuclear Plant: Reactor Vessel Nozzle to Pipe Weld Regions", WCAP-15615, December 2000.

G.14 F. W. Brust, P. Dong, J. Zhang, "Influence of Residual Stresses and Weld Repairs on Pipe Fracture", Approximate Methods in the Design and Analysis of Pressure Vessels and Piping Components, W. J. Bees, Ed., PVP-Vol. 347, pp. 173-191, 1997.

G.15 J. Zhang, P. Dong, F. W. Brust, W. J. Shack, M. Mayfield, M. McNeil, "Modeling of Weld Residual Stresses in Core Shroud Structures", International Journal for Nuclear Engineering and Design, Volume 195, pp. 171-187, 2000.

G.16 Brust, F. W., and Dong, P., "Welding Residual Stresses and Effects on Fracture in Pressure Vessel and Piping Components: A Millennium Review and Beyond", Transactions of ASME, Journal Of Pressure Vessel Technology, Volume 122, No. 3, August 2000, pp. 329-339.